Eur. Phys. J. D (2012) 66: 117
DOI: 10.1140/epjd/e2012-20707-3

THE EUROPEAN PHYSICAL JOURNAL D

Regular Article

Periodic structures in the Franck-Hertz experiment with neon: Boltzmann equation and Monte-Carlo analysis

R.D. White[1,a], R.E. Robson[1], P. Nicoletopoulos[2], and S. Dujko[3]

[1] ARC Centre for Antimatter-Matter Studies, School of Engineering and Physical Sciences, James Cook University, 4810 Townsville, Australia
[2] Faculté des Sciences, Université Libre de Bruxelles, 1050 Brussels, Belgium
[3] Institute of Physics, University of Belgrade, Zemun, 11080 Belgrade, Serbia

Received 6 December 2011 / Received in final form 27 February 2012
Published online 17 May 2012 – © EDP Sciences, Società Italiana di Fisica, Springer-Verlag 2012

Abstract. The Franck-Hertz experiment with neon gas is modelled as an idealised steady-state Townsend experiment and analysed theoretically using (a) multi-term solution of Boltzmann equation and (b) Monte-Carlo simulation. Theoretical electron periodic electron structures, together with the 'window' of reduced fields in which they occur, are compared with experiment, and it is explained why it is necessary to account for all competing scattering processes in order to explain the observed experimental 'wavelength'. The study highlights the fundamental flaws in trying to explain the observations in terms of a single, assumed dominant electronic excitation process, as is the case in text books and the myriad of misleading web sites.

1 Introduction

1.1 The experiment and its interpretation

The quantized nature of atomic energy levels was confirmed in 1914 through the seminal experiment of Franck and Hertz [1] involving electrons drifting in a vapour of mercury atoms in response to an applied voltage. Details of the experimental arrangement can be found in standard text books (e.g. [2]), articles [3–7] and numerous dedicated web sites, and commercial off the shelf Franck-Hertz tubes (see e.g. [8]) can readily be obtained for the undergraduate laboratory, with various gases filling the tube. However, generally speaking, the proliferation in availability of hardware has not been matched by any corresponding enlightenment of the underlying physics. Quite the opposite in fact: the traditional description omits, oversimplifies or downright misrepresents what really happens in the Franck-Hertz drift tube, and otherwise does not do justice to the brilliance of the experimental design. Nowhere is the problem more evident that for neon gas, the focus of the present article.

The key to the operation of the experiment is the formation of a periodic structure within the drift tube, with a wavelength determined by the quantized energy *levels* (not just a single level) of the atom. This periodic profile is projected onto an external circuit through the agency of a third (grid) electrode placed between the cathode and the anode. While there may be questions about the intrusive nature of this grid, i.e., whether it perturbs the phenomenon under investigation, it is the generally poor understanding of the periodic structure itself which is of greatest concern. Thus representation of the electrons in terms of a mono-energetic, unidirectional beam, influenced by a single quantized level of the atom, leading to a uniform, saw tooth structure (see figure 6 of [6]), is completely incorrect, both qualitatively and quantitatively. Quite the opposite situation prevails in fact: electron velocities are randomized by elastic collisions, resulting in an almost isotropic distribution of velocities. The broad range of electron energies means several inelastic channels are open simultaneously, and the wavelength of the periodic structure is therefore generally determined by a composite of several quantized states of the atom, not just one. The periodic structure is smoothly varying, not sawtooth, and is uniform only sufficiently far downstream from the source. Put another way, the influence of the source may extend over a distance corresponding to a number of wavelengths, and the anode should therefore not be too close to the source. Another operational consideration is that periodic structures form, and therefore the experiment can operate, only within a certain window of voltages and gas pressures. The traditional argument has nothing to say on these matters, and neither do crude mean free path arguments [6]. The richness and complexity of the physics associated with the electrons in a Franck-Hertz drift tube, and the conditions for satisfactory operations, can be best understood with any rigour only within the context of modern gaseous

[a] e-mail: ronald.white@jcu.edu.au

electronics. The literature on this approach has been developed for more than a decade, but is still to be accepted by the physics community at large. The three methods of gaseous electronics involve:

– accurate numerical solutions of the Boltzmann kinetic equation;
– Monte-Carlo simulation; and
– fluid modelling.

This paper discusses the first two methods for neon gas. Our own experimental results are given for ease of reference and for the sake of completeness, and to highlight the dangers of trying to understand the observations on the basis of an incorrect physical model. In many ways, the Franck-Hertz experiment with neon, as discussed here, highlights most clearly everything that is wrong with the traditional explanation given in the literature.

We emphasize that there is no question whatever that the Franck-Hertz experiment confirmed the existence of quantised atomic energy levels. Rather, our aim is to understand more rigorously how that quantization emerges in experiment, and to promote a more up to date way of understanding the inherently rich physics.

1.2 Periodic structures in gaseous electronics

It is interesting to note that oscillations of the Franck-Hertz type are actually ubiquitous in gaseous electronics, for example in striations [9], Holst-Oosterhuis luminous layers [10], steady-state Townsend experiment observations using the photon flux technique [11] and periodic structures in low temperature plasmas [7,12–14]. The underlying physics is similar in all cases though the connection with the original Franck-Hertz experiment is not always acknowledged.

The method of sampling the wavelength in the Franck-Hertz experiment involves the insertion of a grid electrode, which almost certainly perturbs the structure. A non-intrusive method of observation, such as the photon flux technique reported by Fletcher [11], offers a far more satisfactory means of sampling periodic structures. In fact, in what follows we refer to Fletcher's results for neon in order to resolve an anomaly in the measured Franck-Hertz current-voltage profile, which we think may be caused by the grid itself.

1.3 Outine of this article

The outline of this article is as follows: in Section 2 we give a brief description of the Franck-Hertz experiment for neon and some results for a commercially available drift tube, along with the traditional interpretation. In Section 3, we explain the way in which microscopic, atomic properties, like cross-sections and threshold energies, are reflected in macroscopically measurable quantities, like the anode current, using both kinetic theory, specifically the Boltzmann equation, and Monte-Carlo simulation. A brief discussion of a multi-term spherical harmonic/eigenfunction solution of the Boltzmann equation [4], along with a Monte-Carlo simulation [15] for the non-equilibrium and non-hydrodynamic evolution of the electron distribution function is presented in Section 3. Section 4 highlights the experimental and operational considerations including how the periodic spatial structures manifest themselves in the I-V characteristics. The two computational methods are examined and compared with each other, and with experiment in Section 5. Particular focus is placed on the interpretation of the results and on the 'window' of reduced fields in which the periodic behaviour is observed.

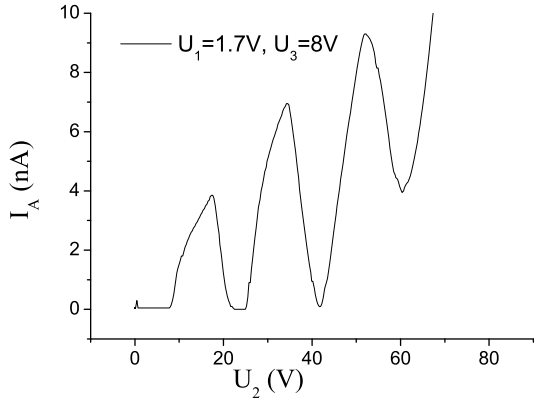

Fig. 1. Measured Franck-Hertz curve for neon using the commercially available Leybold Didactiv GMβH apparatus [8] at room temperature.

2 The Franck-Hertz experiment in neon and common interpretations of the results

In the Franck-Hertz experiment electrons are emitted from a heated cathode, then accelerated firstly by a potential U_1 (between the cathode and the first gate) and secondly by a voltage U_2 (between the first and second gates), with a retarding potential U_3 (between the second gate and the anode). The retarding potential U_3 acts as a control grid only allowing electrons above a certain value to be collected as current at the anode. With a ramping potential U_2, the collected current goes through successive maxima. The periodic structure of the electron distribution functions within the drift tube is reflected in the periodicity in the anode current as a function of U_2. In Figure 1 we present results for neon from a commercially available Franck-Hertz drift tube [8] modelled schematically as in Figure 2. According to the traditional text book interpretation of the Franck-Hertz experiment, electrons are accelerated due to the field (without elastic scattering) until they have sufficient energy to suffer an electronic excitation collision with the neon atom, and the process is repeated until it reaches the anode. This is effectively an assumption of a beam-like distribution of electron velocities, which in turn implies a sawtooth profile of electron properties within the drift tube, of energy wavelength corresponding to the lowest threshold of energy for excitation of the atom, which for neon is 16.6 eV.

The picture of the internal profile should be reflected in the *I-V* characteristic in the external circuit. However, even a cursory analysis of the measured *I-V* profile iin Figure 1 indicates a wavelength of approximately 18 eV, at odds with the prediction of the standard argument. In order to try to salvage the situation, it is often argued that the measurements actually reflect the transition to the $^3S_1$ state, with threshold energy 18.38 eV. Unfortunately it is not clear how or why the electron picks out exactly this state from the multitude of available possible states to excite. The laboratory manual accompanying our system least recognizes that the usual argument must be supplemented with a statement about probability. This view of the relevant physics is probably driven by the observation of visible bands between the two electrodes which are a result of neon atoms excited to the $3p$ states decaying through the $3s$ states through the emission of a visible photon. Nothing is said, however, regarding how or if the effects of the various inelastic channels can be combined, there is no mention of elastic scattering, and the argument is otherwise ad hoc. As is now recognized, any serious physical analysis of the experiment requires the *cross-sections* for each of the scattering processes (elastic and inelastic), and a *distribution function* of energies in order to weight them. The electron distribution function is obtained as a solution of the Boltzmann kinetic equation, which incorporates the cross-sections for the scattering processes. Electron properties within the drift tube are then calculated as averages over the distribution function, and all processes, both elastic and inelastic, are accounted for rigorously. That is the approach outlined in 2000 by Robson et al. [4], initially for mercury, but applicable to any gas. Monte-Carlo simulation, in which the averaging is done directly, provides an alternative rigorous picture. Both are discussed in this article in the context of neon gas, as detailed below.

3 Theoretical treatments and simulations

3.1 Kinetic theory treatment: Multi-term eigenfunction solution of the Boltzmann equation

The governing equation describing a swarm of free light charged particles moving through a gas under the application of an electric field $\boldsymbol{E}$ under steady state conditions is the time-independent Boltzmann equation for the phase space distribution function $f(\boldsymbol{r},\boldsymbol{c})$ [16]:

$$\boldsymbol{c}\cdot\nabla f+\frac{q\boldsymbol{E}}{m}\cdot\frac{\partial f}{\partial\boldsymbol{c}}=-J(f). \tag{1}$$

Here $\boldsymbol{r}$ and $\boldsymbol{c}$ denote respectively the position and velocity coordinates in phase space while q and m are the charge and mass of the particle respectively. The collision operator J describes the rate of change of f due to binary interactions with the background gas and for elastic processes we utilise the original Boltzmann collision operator [16] while for inelastic processes such as electronic excitation we implement the semi-classical generalisation of Wang-Chang et al. [17]. For ionization processes we implement the ionization collision operator detailed in [18].

Solution of the Boltzmann equation (1) requires representation of the space and velocity dependence of $f(\boldsymbol{r},\boldsymbol{c})$. Below we present a brief discussion on the relevant representations.

3.1.1 Treatment of the velocity dependence: Multi-term spherical harmonic expansion

The first step in any analysis is typically the representation of the distribution function in directions of velocity space through an expansion in spherical harmonics [19]:

$$f(\boldsymbol{r},\boldsymbol{c})=\sum_{l=0}^{\infty}\sum_{m=-l}^{l}f_m^{(l)}(\boldsymbol{r},c)Y_m^{[l]}(\hat{\boldsymbol{c}})\,, \tag{2}$$

where $Y_m^{[l]}(\hat{\boldsymbol{c}})$ are spherical harmonics and $\hat{\boldsymbol{c}}$ denotes the angles of $\boldsymbol{c}$. While it is traditional (in the two-term approximation) to set the upper bound of the l-summation to 1 and set $m=0$ (i.e. a Legendre polynomial expansion), we do not make such a restrictive assumption in this theory.

Various numerical techniques are applicable to represent the speed/energy space [19,20]. In this paper we employ an expansion in terms of generalised Sonine (generalised Laguerre) $R_{\nu l}(\alpha c)$ polynomials [21]:

$$f_m^{(l)}(\boldsymbol{r},c)=w(\alpha,c)\sum_{\nu=0}^{\infty}F_\alpha(\nu lm;\boldsymbol{r})R_{\nu l}(\alpha c), \tag{3}$$

which are orthonormal with respect to a Maxwellian weight function $w(\alpha,c)=(\frac{\alpha^2}{2\pi})^{3/2}\exp\{\frac{-\alpha^2c^2}{2}\}$, where $\alpha^2=m/kT_b$. The parameter T_b is chosen to be the charged-particle temperature or an arbitrary basis temperature [22]. These are traditionally referred to as the 'two-temperature theory' [18,22].

Substituting (2) and (3) into (1), and utilising the orthonormality of the basis functions, we obtain the following infinite set of partial differential equations for the moments $F_\alpha(\nu lm;\boldsymbol{r})$:

$$\sum_{\nu'=0}^{\infty}\sum_{l'=0}^{\infty}\sum_{m'=-l'}^{l'}\left[\langle\nu lm||J+\frac{q\boldsymbol{E}}{m}\cdot\frac{\partial}{\partial\boldsymbol{c}}+\boldsymbol{c}\cdot\nabla||\nu'l'm'\rangle\right]\times F_\alpha(\nu lm)=0 \tag{4}$$

where $\langle\nu lm||J+\frac{q\boldsymbol{E}}{m}\cdot\frac{\partial}{\partial\boldsymbol{c}}+\boldsymbol{c}\cdot\nabla||\nu'l'm'\rangle$ are matrix elements of the collision and streaming operators [18].

3.1.2 Treatment of the spatial dependence: Eigenfunction expansion in the non-hydrodynamic regime

The Franck-Hertz experiment is specifically a non-hydrodynamic phenomena. For the steady state and plane parallel conditions in the prototype model considered here,

there is a source of electrons from $z = z_0$ emitted at a constant rate with a velocity distribution $S(c)$. The problem is completed by specifying the boundary conditions on f at the electrodes. For the semi-infinite half-plane problem under consideration here, the details for prescribing the boundary conditions are found in [4,23,24] but essentially amount specifying components of the source distribution (spherical harmonic projections $f_m^{(l)}(\boldsymbol{r}, c)$) at $z = z_0$, and requiring certain conditions on the phase-space distribution function at infinity. The simplest technique is a discretisation in space (e.g. finite difference or pseudo-spectral method) requiring however a computationally demanding solution of large system of coupled matrix equations [4,24,25]. The spatial relaxation behaviour is influenced by the source distribution in addition to the field and scattering processes of the gas. At sufficiently large distances from the source however, the impact of the source distribution is lost and the relaxation behaviour of the electrons is representative of the electron-atomic scattering processes within the gas. Hence the focus of the current Boltzmann equation analysis is on the asymptotic relaxation of the distribution function and its moments to their respective equilibrium values. To elucidate the basic physics, we prefer to adopt the eigenfunction methodology developed in [4,23]. The eigenvalue equation associated with the spherical harmonic decomposition (4) is given by:

$$\sum_{\nu'=0}^{\infty}\sum_{l'=0}^{\infty}\sum_{m'=-l'}^{l'}\left[\langle \nu l m||J + \frac{qE_z}{m}\frac{\partial}{\partial c_z} + c_z K||\nu' l' m'\rangle\right] \times \psi(\nu l m;\alpha) = 0 \quad (5)$$

where K is the eigenvalue and ψ is the corresponding eigenfunction. The spectrum of eigenvalues is generally discrete, with a representation $\{K_n,\ n = 0, 1, 2, \ldots\}$ (assumed order such that the $|\mathrm{Re}\,(K_n)\,|$ increases with n) and associated eigenfunctions $\{\psi_n,\ n = 0, 1, 2, \ldots\}$. Asymptotically the system approaches the state ψ_0 determined by the eigenfunction associated with the eigenvalue K_0, i.e. $f \sim \exp(K_0 z)$, and K_0 is the first Townend coefficient. While all eigenmodes contribute to the spatial behaviour for the general problem, for the semi-infinite half-plane problem under consideration, in the downstream asymptotic regime only those K_n $(n > 0)$ with a non-negative real component satisfy the upper boundary condition at infinity. The rate at which the state is approached is controlled by the eigenvalue with lowest magnitude negative real component, K_1. This eigenvalue will play a significant role in elucidating the fundamental physics associated with the Franck-Hertz experiment in neon.

The spatial dependence of the phase-space distribution function and associated integral properties of interest can be expressed in the asymptotic limit as a series [4,23], e.g. the mean energy

$$\epsilon(z) = \frac{\int \frac{1}{2}mc^2 f(z,\boldsymbol{c})d\boldsymbol{c}}{\int f(z,\boldsymbol{c})d\boldsymbol{c}} = \epsilon_\infty + \epsilon_1 \exp\left(K_1(z - z_0)\right) + \ldots \quad (6)$$

where ϵ_∞ is the asymptotic value of the average energy. For elastic collisions only, K_1 is real and the spatial development is monotonic relaxation to the asymptotic state. When K_1 becomes complex however the spatial development has an oscillatory nature, with a wavelength $\Delta z = 2\pi/\mathrm{Im}(K_1)$, and a characteristic relaxation length Λ of $1/|\mathrm{Re}(K_1)|$. The reader is referred to [4,23] for details on the implementation and calculation of the eigenvalues and eigenfunctions. This procedure has been benchmarked against models for which the eigenvalues and eigenfunctions are known analytically [4,23].

3.2 Monte-Carlo simulation treatment

The Monte-Carlo simulation technique used to evaluate the spatial profiles under steady-state Townsend conditions has been detailed elsewhere [15] and we will highlight briefly the important aspects of the simulation. In this Monte-Carlo simulation code electrons are ejected isotropically and sequentially from the cathode (filament) surface into the infinite half space with an initial energy distribution. The trajectories of a large number of electrons are followed under the influence of an electric field as they undergo collisions with background neon atoms. The electron's motion is sampled at sufficiently high frequency (determined by the mean collision time) to find the time to next collision via direct numerical integration of the integral equation for the collision probability [26]. Once the moment of the next collision is established, the nature of the collision is determined by using the relative probabilities of the various collision types [15,27,28]. When an ionization collision occurs, the set of all dynamic properties (the time of the ionization collision, the position and velocity) of secondary/ejected electron are placed at the stack. When the primary electron reaches the anode surface or is otherwise lost in a collision event, the first available electron from the stack is then followed. These secondary electrons from the stack are assumed to be released isotropically although facility exists to enforce a specified angular distribution. Thermal motion of the background neutral particles and electron-electron interactions are neglected. The electrodes are considered to be perfectly absorbing. To obtain the spatially resolved steady state profiles, further manipulation of the Monte-Carlo sampling of the phase-space distribution function $f(\boldsymbol{r}, \boldsymbol{c}, t)$ is required. We may interpret the distribution function as a sum of Dirac delta functions:

$$f(\boldsymbol{r}, \boldsymbol{c}, t) = \sum_{k=1}^{N(t)} \delta\left(\boldsymbol{r}_k(t) - \boldsymbol{r}\right)\delta\left(\boldsymbol{c}_k(t) - \boldsymbol{c}\right) \quad (7)$$

where $N(t)$ is the number of electrons at time t. To obtain the steady-state distribution function $f(\boldsymbol{r}, \boldsymbol{c})$ we integrate (7) over all time [15]. With the steady-state distribution function, one then may evaluate the spatially resolved steady state profile through the relevant discretization (boxing) in space and associated averages over velocity and remaining configuration space. For example, the

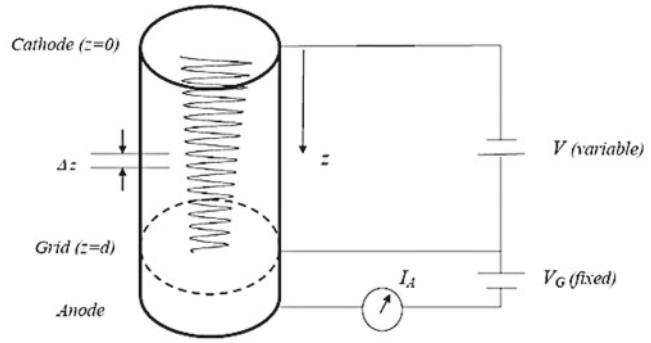

Fig. 2. Schematic representation of the Franck-Hertz experiment, in which a steady stream of electrons emitted by the cathode into a gas forms a macroscopic periodic structure of wavelength Δz in the drift region $0 \leq z \leq d$, reflecting quantization of gas atoms. In the idealized model of standard arguments, where atoms have a single, quantized level of energy ϵ_I, $\Delta z = \epsilon_I d/\mathrm{eV}$, where d is the distance to the control grid, which is at a potential V with respect to the cathode. As V increases, the periodic pattern shrinks, and the current I_A in the external circuit goes through a series of maxima and minima, resulting in an oscillatory I_A-V characteristic of 'wavelength' $\Delta V = \epsilon_I/e$. In reality, however, the picture is far more complicated, since atoms have more than one quantized level, many scattering channels are open simultaneously, and ΔV cannot be simply represented in terms of any single energy level.

mean energy in the jth box (i.e. between $z_j - \Delta z/2$ and $z_j + \Delta z/2$) has been calculated as follows:

$$\begin{aligned}\langle\varepsilon\rangle_j &= \left(\frac{1}{\Delta z}\int_{z_j-\Delta z/2}^{z_j+\Delta z/2} \varepsilon f_{\mathrm{SST}}(z,\boldsymbol{v})d\boldsymbol{r}d\boldsymbol{v}\right)^{-1} \\ &\quad\times \frac{1}{\Delta z}\int_{z_j-\Delta z/2}^{z_j+\Delta z/2} f_{\mathrm{SST}}(z,\boldsymbol{v})d\boldsymbol{r}d\boldsymbol{v} \\ &\approx \left(\sum_{k=1}^{N}\Delta t_k^j\right)^{-1}\sum_{k=1}^{N}\varepsilon_k^j\Delta t_k^j\,, \end{aligned} \tag{8}$$

where $f_{\mathrm{SST}}(z,\boldsymbol{v})$ is the steady state distribution function, ε_k^j is the value of the mean energy to be sampled when the kth electron is contained in jth box, Δt_k^j is the residence time of the electron in that box, Δz is the width of the box, and N is the total number of electrons which appear there. For details the reader is referred to [15].

4 Experimental considerations

4.1 Schematic representation of the experiment

A schematic representation of an idealised Franck-Hertz experiment is displayed in Figure 2. We have a source of electrons emitted from $z = 0$ into the neon gas occupying the space between the electrodes. This is equivalent to a steady-state. Townsend experiment common in swarm physics [29]. The electric field is assumed to be constant and uniform between the two parallel plate electrodes. For the current study it is sufficient to focus on the semi-infinite geometry and consider the electrode to approach infinity. In the real Franck-Hertz experiment there is a control grid downstream from the source which selectively filters electrons above a prescribed energy to be collected by the anode and register as a current.

4.2 External I-V curve vs. internal periodic structure

It is axiomatic that the act of measurement should not affect the quantity being measured. In the case of the Franck-Hertz experiment, the grid should act in a non-intrusive way, without perturbing the quantity being sampled, namely, the periodic electron structure which forms between the cathode and the grid. Thus the I-V characteristic projected onto the external circuit should be in one-to-one correspondence with the internal profile, at least to within experimental error. However, as explained below, there is a violation, both qualitative and quantitative, of this basic precept for the Franck-Hertz experiment with neon. In particular, we suggest that the substructure near the minima in the I-V profile shown in Figure 1 is not a reflection of the internal profile because:

(a) There is no such substructure evident in the direct, non-intrusive measurements of Fletcher [11] of the electron profile in the steady state Townsend experiment (effectively the Franck-Hertz experiment without a grid) for neon, or indeed any other gas.
(b) Neither does any such substructure appear in the periodic profile calculated theoretically using either rigorous solution of the Boltzmann equation or Monte-Carlo simulation, (see Figs. 4-6 below): the profile is smoothly varying everywhere, and characterised by a single, distinctive wavelength at sufficiently large distances from the source.

We therefore suggest that the substructure in the I-V profile for neon is an artefact of the measurement process, most probably due to the perturbative nature of the grid. A direct way of establishing this would be to let $V_G \to 0$ (or equivalently $U_3 \to 0$ in the terminology of the commercial equipment [8]), and indeed our own data suggest that the substructure weakens considerably in this limit. Whatever its origin, the substructure of the I-V should be discounted as reflecting any sort of quantization property of the neon atom, and attention should be focussed on the main structure, with voltage V (or U_2 as used in [8]). Note that while the determination of an accurate value of ΔV is a prime experimental consideration, its interpretation in terms of the spectrum of excited energy levels of the atom is a separate theoretical matter, as discussed further[1] in Section 5.

[1] This is diametrically opposed to the conclusions of Rapior et al. [6], who however base their arguments on an assumed but unphysical sawtooth periodic structure, with perturbations calculated from simplified mean free path arguments and a constant cross-section.

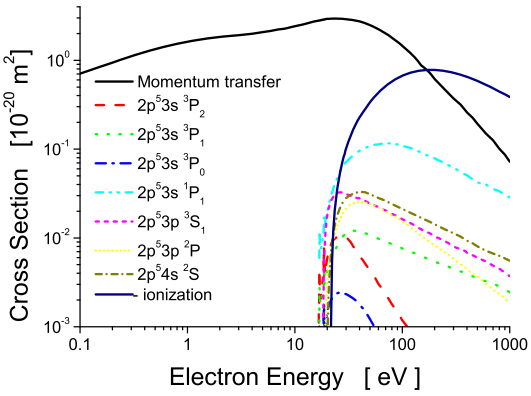

Fig. 3. (Color online) The electron impact cross-sections for neon. We employ a momentum transfer cross-section for elastic processes while the inelastic and ionization processes are assumed isotropic (see text for details).

4.3 Operational considerations

There are two basic factors crucial to the successful operation of the Franck-Hertz experiment for any gas, neon in particular. These are either ignored completely or simply inexplicable in terms of the standard, unphysical 'saw tooth' profile argument:

(a) A periodic structure can form in the drift tube and the experiment can therefore operate satisfactorily, only within a well defined window of voltages and gas pressures. This is discussed further for neon in Section 5.2.

(b) The influence of the source may extend some way downstream, and a pattern characterized by a single, fundamental wavelength, characteristic of the gas only, becomes established only after a certain relaxation distance. The drift region must obviously be longer than this distance, so that the grid falls in the asymptotic region, for otherwise the external I-V curve will be contaminated by the influence of the source. The relaxation distance and the fundamental wavelength can be found from eigenvalue analysis of the Boltzmann equation (see Sect. 5.2 below). For practical purposes, however, simply ensuring that several oscillations exist in the drift tube should be sufficient to guarantee satisfactory interpretation of the experiment in terms of a single fundamental energy wavelength ϵ_f, i.e., an operational criterion is $V > \epsilon_f$. This is the situation shown in Section 5.2. Since ϵ_f is around 18 V for neon, it is meaningful to try to extract fundamental information only at voltages substantially in excess of this.

5 Results and discussion

5.1 Experimental configuration, input cross-sections and scalings

In this study we employ the set of cross-sections for electrons in neon prescribed by Hayashi [30] and presented in Figure 3. These cross-sections are based on the benchmarked set of [31] which were extended to higher energies and benchmarked in [32]. Elastic scattering is anisotropic in nature as described by the momentum transfer cross-section, while all non-elastic cross-sections are assumed isotropic. The temperature is fixed at 293 K. Since the collision operator is proportional to the number density n_0, the spatial position scales as $n_0 z$, while the eigenvalues scale as K_n/n_0. In what follows we present quantities scaled by a representative mean free path $\lambda = 1/\left(\sqrt{2} n_0 \sigma_0\right)$ where $\sigma_0 = 10^{-20}$ m^2. Likewise all transport properties are functions of the reduced electric field E/n_0. We consider the reduced electric field range: 1−100 Td (1 Td $= 10^{-21}$ V m^2).

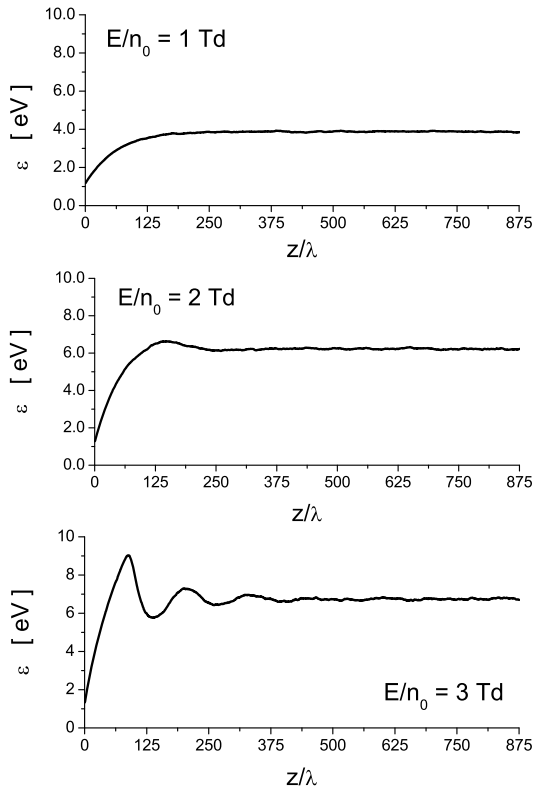

Fig. 4. Spatial relaxation of electrons in neon simulated using a Monte-Carlo simulation technique (top: 1 Td; middle: 2 Td; bottom: 3 Td).

5.2 Spatial relaxation profiles in neon: Relaxation lengths and windows for oscillatory relaxation

In this Section we focus on the general properties of the relaxation profiles for electrons injected in neon gas under the action of an applied spatially homogeneous electric field. In Figures 4−6 we display the MC simulated relaxation profiles for the average energy of electrons released with a mono-energetic distribution at 1 eV into neon gas under the action of an applied field ranging from 1 Td to 60 Td. Although only profiles of the average energy are displayed here, the same qualitative behaviour is present for all other macroscopic properties such as the number density and the average velocity. For reduced fields below

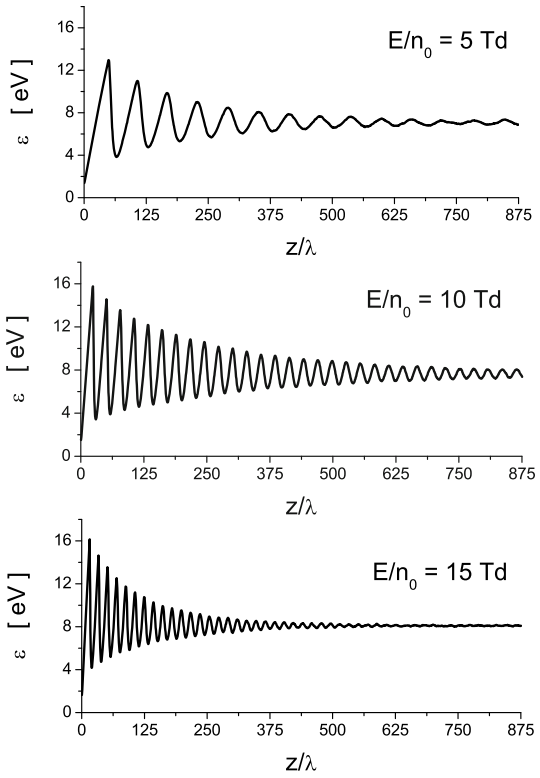

Fig. 5. Spatial relaxation of electrons in neon simulated using a Monte-Carlo simulation technique (top: $E/n_0 = 5$ Td; middle: 10 Td; bottom: 15 Td).

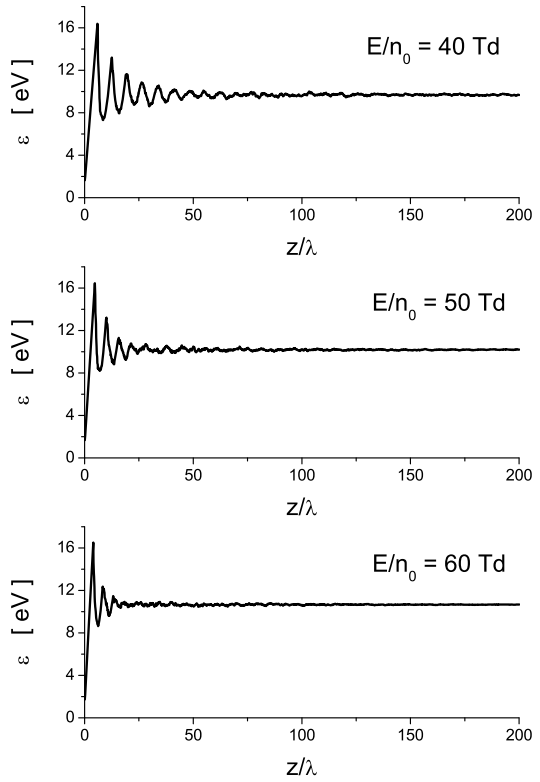

Fig. 6. Spatial relaxation of electrons in neon simulated using a Monte-Carlo simulation technique (top: 40 Td; middle: 50 Td; bottom: 60 Td).

2 Td, we observe that the relaxation behaviour is monotonic. As we increase the field however, we observe as expected, that a window of field strengths exists where the relaxation behaviour is (damped) oscillatory in nature. We will defer a discussion of the wavelength of the oscillations to Section 5.3. The upper bound on the window of oscillatory relaxation (not shown here) is approximately 300 Td where relaxation returns to a monotonic/quasi-monotonic nature.

In these profiles we observe that the distance required for the transport properties to relax to their asymptotic steady states varies with the applied reduced field. The relaxation distance has a maximal property with the largest relaxation distance appearing around 10 Td. The relaxation distance is drastically reduced at high fields (note the change of scale in Fig. 6).

The relaxation profiles in neon are consistent with the previous discussions on this topic [4,5,24,33] and consistent with the experimental results presented in Section 2. The periodic nature in the collector current as a function of the ramped voltage can be related to the spatial structure of the average energy of the electrons within the drift tube. For reduced field strengths such that the electronic excitation modes can not be excited, energy loss due to collisions is via elastic collisions and is essentially continuous, and the monotonic/quasi-monotonic nature of the relaxation profiles then follow. For field strengths such that energy loss via electronic excitation is significant, the discrete nature of the energy loss in this regime results in the periodic behaviour in the relaxation profiles. The decaying nature of the oscillatory profiles is primarily determined by the elastic scattering processes [4,24].

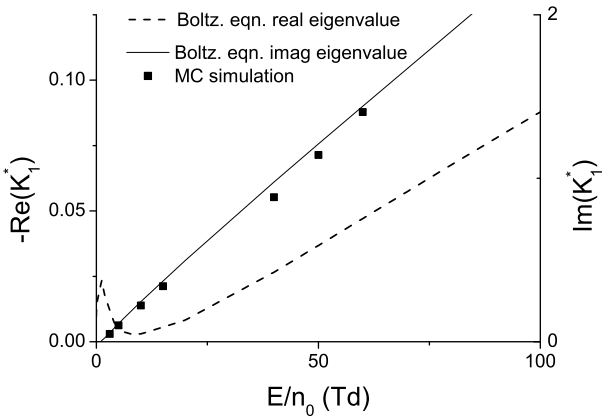

Fig. 7. Variation with reduced electric field of the real and imaginary components of the eigenvalues (or equivalent) corresponding to the asymptotic behaviour. The normalized eigenvalues $K_1^* = K_1\lambda$, where $\lambda = \sqrt{2}n_0\sigma_0$ is a representative mean free path used to scale the eigenvalues.

5.3 Eigenvalue governing the asymptotic behaviour

In Figure 7 we present the real and imaginary parts of the reduced eigenvalue K_1^* which govern the

asymptotic relaxation to the steady-state. In the multi-term Boltzmann equation calculation of this eigenvalue, we have made an assumption to treat ionization as an inelastic process (i.e. we neglect the ejected electron). We observe that K_1^* is complex for reduced fields greater than approximately 1.2 Td which is consistent with the the behaviour demonstrated in the Monte-Carlo profiles of Figures 4–6. Using traditional arguments, the spacing between successive peaks should be given by the relation $eE\Delta z = \epsilon_I$, where ϵ_I is a representative threshold energy. Hence, theoretically the relevant reduced eigenvalue should have the following functional form:

$$\mathrm{Im}\,(K_1^*) = \frac{2\pi(E/n_0)_{\mathrm{Td}}}{10\sqrt{2}\epsilon_I(\mathrm{eV})}. \tag{9}$$

Examination of Figure 7 highlights that the imaginary part of K_1^* is approximately proportional to the reduced electric field strength E/n_0 for those reduced fields in the window. The relaxation length associated with the asymptotic relaxation is determined by the renormalised relaxation length $\Lambda^* = 1/|\mathrm{Re}(K_1^*)|$. The maximal property in the relaxation length is observed at approximately 8 Td with a significantly reduced relaxation length at higher reduced fields. Again, the behaviour of the real component is qualitatively consistent with the profiles in Figures 4–6.

5.4 Wavelengths, threshold energies and interpretation

In this section we investigate the relation between the wavelength of the spatially periodic structures in the energy profiles and the representative 'threshold energy' of the electronic excitation process. Using a fast Fourier transform, we have extracted the relevant asymptotic wavelengths from the Monte-Carlo profiles and scaled them for comparison with reduced eigenvalue K_1^*. The results are presented in Figure 7. The results are qualitatively similar however for a given field the wavelength calculated using the Monte-Carlo simulation is larger (or equivalently $\mathrm{Im}(K_1^*)$ is smaller) than that from the Boltzmann equation eigenvalue theory. More generally, the wavelength is longer when we treat ionization as a true non-conservative process. This result is consistent with the physics of the problem: in a true ionization event, the excess energy is now shared between the ejected and scattered electron. Hence, on average the scattered and ejected electrons must travel further in the field in order to have sufficient energy to overcome the excitation threshold energy. The increase in the wavelength associated with treating ionization explicitly then follows [15,24].

Using the traditional textbook interpretation of the Franck-Hertz experiment, these results could be interpreted as different representative threshold energies ϵ_I for the two different techniques. Using least squares to fit the wavelength of the spatially periodic structures to a representative threshold energy via equation (9), we find that the Boltzmann equation eigenvalue theory predicts a representative threshold energy of 18.78 ± 0.06 eV while the Monte-Carlo simulation predicts a representative threshold energy of 19.0 ± 0.2 eV. This should be compared with the approximate experimental result of 18 eV. It is instructive at this time to compare these values with the actual thresholds for the various collision induced processes processes in neon as detailed in Table 1. As discussed in Section 2, using the most elementary of traditional textbook interpretations of the Franck-Hertz experiment, one might expect a wavelength associated with the lowest ^{3}P excitation threshold 16.62 eV threshold. With a knowledge of the magnitudes of the various cross-sections, the wavelength might naturally be associated with the ^{1}P 16.85 eV electronic excitation process, or possibly more accurately as the ionization threshold process at 21.56 eV.

Table 1. Threshold energies and approximate maximum cross-sections for the various electron induced processes in neon [30].

Process	Threshold (eV)	Maximum cross-section (10^{-20} m^2)
$2p^5 3s\ ^3\mathrm{P}_2$	16.62	0.01
$2p^5 3s\ ^3\mathrm{P}_1$	16.67	0.012
$2p^5 3s\ ^3\mathrm{P}_0$	16.72	0.0024
$2p^5 3s\ ^1\mathrm{P}_1$	16.85	0.12
$2p^5 3p\ ^3\mathrm{S}_1$	18.38	0.033
$2p^5 3p\ ^2\mathrm{P}$	18.97	0.026
$2p^5 4s\ ^2\mathrm{S}$	19.66	0.033
Ionization	21.56	0.78

The results presented here, both experimental and theoretical/simulation, indicate that threshold energy information can not be inferred directly from the wavelength of the periodic structures when there are excitation processes with closely spaced threshold energies and cross-sections magnitudes of the same order. The distribution of energies of the electrons within the drift chamber means that all scattering processes listed in Table 1 are open for reduced electric fields above the lower bound of the window. In particular, one may associate the periodic structures present in the profiles as representative of some weighted average of the various inelastic processes available. For neon considered here, the dominant contributions are from the two largest cross-sections, ^{1}P electronic excitations and the ionization processes, with 16.85 eV and 21.56 eV threshold energies respectively. The relative excitation rates for the various excitation/ionization processes will vary with the applied field. We must emphasize that it is incorrect to interpret the 18 eV experimental result to mean that the excitation to the $2p^5 3p\ ^3\mathrm{S}_1$ (with threshold of approximately 18 eV) is the dominant process reflected in the Franck-Hertz profiles.

6 Concluding remarks

In this study we have investigated the Franck-Hertz experiment for neon, using a commercially available drift tube, and have focussed on rigorous interpretation of the current-voltage characteristic in the external circuit in terms of the periodic electron structure within the Franck-Hertz drift tube. The internal profile has been calculated theoretically using electron-neon atom scattering cross-sections in two distinct ways: (a) Accurate solution of

Boltzmann's kinetic equation; and (b) Monte-Carlo simulation. All open scattering channels, both elastic and inelastic, are accounted for rigorously in both these approaches, in contrast to the standard, but physically untenable picture of a beam of electrons, in which only a single inelastic channel is open, and all others are artificially suppressed. The rigorous methods discussed in this article produce smoothly varying curves, with wavelengths in good agreement with experimental results. Substructures are, however, not observed in the theoretical profiles, and evidence is advanced to explain why these are due to the perturbative influence of the grid, rather than any fundamental properties of the atoms per se.

The support of the Australian Research Council is gratefully acknowledged. This research is also funded in part by Belgium Science policy under contract IAP VI/11 and by IISN. We would also like to thank Prof. R. McEachran and Prof. Y. Namakmura for their valuable input.

References

1. J. Franck, G. Hertz, Verh. Deutsche Phys. Ges. **16**, 457 (1914)
2. R.A. Serway, C.J. Moses, C.A. Moyer, *Modern Physics* (Thomson Learning, Belmont, 2005)
3. G.F. Hanne, Am. J. Phys. **56**, 696 (1988)
4. R.E. Robson, B. Li, R.D. White, J. Phys. B: At. Mol. Opt. Phys. **33**, 507 (2000)
5. F. Sigeneger, R. Winkler, R.E. Robson, Contrib. Plasma Phys. **43**, 178 (2003)
6. G. Rapior, K. Sengstock, V. Baev, Am. J. Phys. **74**, 423 (2006)
7. P. Nicoletopoulos, R.E. Robson, Phys. Rev. Lett. **100**, 124502 (2008)
8. Leybold physics leaflets: Atomic shell Franck-Hertz experiment p6.2.4.4, http://www.ld-didactic.de/literatur/hb/e/p6/p6243_e.pdf
9. A. Muller, Nature **157**, 119 (1946)
10. G. Holst, E. Oosterhuis, Physica **1**, 78 (1921)
11. J. Fletcher, J. Phys. D **18**, 221 (1985)
12. Yu.B. Golubovskii, A.Yu. Skoblo, C. Wilke, R.V. Kozakov, J. Behnke, V.O. Nekutchaev, Phys. Rev. E **72**, 026414 (2005)
13. V.I. Kolobov, J. Phys. D **39**, R487 (2006)
14. Yu.B. Golubovskii, A.Yu. Skoblo, C. Wilke, R.V. Kozakov, V.O. Nekuchaev, Plasma Sources Sci. Technol. **18**, 045022 (2009)
15. S. Dujko, R.D. White, Z.Lj. Petrović, J. Phys. D **41**, 245205 (2008)
16. L. Boltzmann, Wein. Ber. **66**, 275 (1872)
17. C.S. Wang-Chang, G.E. Uhlenbeck, J. De Boer, in *Studies in Statistical Mechanics*, edited by J. De Boer, G.E. Uhlenbeck (Wiley, New York, 1964), Vol. II, p. 241
18. K.F. Ness, R.E. Robson, Phys. Rev. A **34**, 2185 (1986)
19. R.E. Robson, K.F. Ness, Phys. Rev. A **33**, 2068 (1986)
20. E.A. Mason, E.W. McDaniel, *Transport Properties of Ions in Gases* (Wiley, New York, 1988)
21. S. Chapman, T.G. Cowling, *The mathematical theory of non-uniform gases* (Cambridge University Press, Cambridge, 1939)
22. S.L. Lin, R.E. Robson, E.A. Mason, J. Chem. Phys. **71**, 3483 (1979)
23. B. Li, *Hydrodynamic and non-hydrodynamic charged particle swarms*, Ph.D. thesis, James Cook University, 1999
24. B. Li, R.D. White, R.E. Robson, J. Phys. D **35**, 2914 (2002)
25. G. Petrov, R. Winkler, J. Phys. D **30**, 53 (1997)
26. H. Itoh, T. Musha, J. Phys. Soc. Jpn **15**, 1675 (1960)
27. S. Bzenić, Z.M. Raspopović, S. Sakadžić, Z.Lj. Petrović, IEEE. Trans. Plasma Sci. **27**, 78 (1999)
28. H.R. Skullerud, J. Phys. D **1**, 1567 (1968)
29. L.G.H. Huxley, R.W. Crompton, *The Drift and Diffusion of Electrons in Gases* (Wiley, New York, 1974)
30. M. Hayashi, private communication, 2000
31. V. Puech, S. Mizzi, J. Phys. **24**, 1974 (1991)
32. Z.D. Nikitovic, A.I. Strinic, V.D. Stojanovic, G.N. Malovc, Z.Lj. Petrovic, Radiat. Phys. Chem. **76**, 556 (2007)
33. F. Sigeneger, R. Winkler, Plasma Chem. Plasma Process. **17**, 281 (1997)